Nappe Oscillations on Free-Overfall Structures: Size Scale Effects

M. Lodomez[1]; B. P. Tullis, F.ASCE[2]; B. Dewals[3]; P. Archambeau[4]; M. Pirotton[5]; and S. Erpicum[6]

Abstract: Nappe oscillation and its potentially undesirable impact associated with significant noise production can be an issue for free-overfall hydraulic structures. Although nappe oscillation has been observed on various prototype free-overfall structures, this instability behavior may not be evident during the design process in which experimental and/or numerical modeling may be utilized. In addition, previous studies regarding nappe oscillation scalability using similitude or other relationships has received very limited attention in the literature. An experimental study aimed at investigating the possible size scale effects on nappe oscillations was undertaken utilizing two experimental facilities: a prototype-scale linear weir (3-m fall height) and a geometrically similar 1:3-scale model (1-m fall height). The nappe oscillation occurrence assessment and oscillation frequency evaluation were performed using sound and image analyses. Experiments on both models showed that the nappe oscillation phenomenon generally occurs over a fixed range of unit discharge and is independent of size scale. Nappe oscillation can therefore not be reproduced at different model scales according to standard similarity laws. This study also highlights the secondary influences of the crest profile and the fall height on the oscillation characteristics. **DOI: 10.1061/(ASCE)HY.1943-7900.0001615.**

Author keywords: Nappe oscillation; Physical modeling; Size scale effect.

Introduction

Nappe oscillation is an instability behavior associated with a gravity-driven free-falling jet occurring under low-head conditions (USBR 1964; MWSDB 1980; Casperson 1993; Chanson 1996; Lodomez et al. 2018c). This instability is characterized by visible horizontal bands, also called waves, that develop across the width of the nappe, and a high noise production sounding something like a helicopter (Casperson 1993). In the case of overflow gates, nappe oscillation can induce vibrations in the structure or its actuators (Lodomez et al. 2018a). The acoustic energy generated by the nappe oscillations may also cause significant negative effects locally such as rattling windows of nearby residences (Crookston et al. 2014). Nappe oscillation behavior has been observed with various prototypes and laboratory-scale physical models. Indeed, they have been observed on fountains, weirs (labyrinth and linear), and gates as referred in Casperson (1993), Crookston et al. (2014), and Lodomez et al. (2018a). In addition, various studies reproduced this unstable behavior using experimental facilities varying significantly in size. Binnie (1972), Sato et al. (2007), and Schmid and Henningson (2002) reported nappe oscillations along 0.3- to 0.7-m-high thin vertical jet issuing from 0.2- to 3-mm-wide pressurized slots, while Anderson and Tullis (2018) and Lodomez et al. (2018c) studied these oscillations on large-scale models of linear weirs, close to typical prototype dimensions.

Despite the development of increasingly accurate numerical models, physical modeling remains a powerful engineering tool to design hydraulic structures and to understand their behavior. Nevertheless, physical modeling remains challenging in that full model-prototype similarity requires that geometric, kinematic, and dynamic similitude be achieved. Using a common fluid (i.e., water) for both prototype and model scales makes full similarity impossible (Ettema et al. 2000), but, in many cases, there is a single dominant force, along with inertia, that justifies neglecting the other minor forces that cannot be accounted for accurately. Particular laws of similitude have been developed based on the ratio of the inertia and other dominant forces [e.g., Froude (gravity), Reynolds (viscosity), and Weber (surface tension)]. Froude similitude is most appropriate, typically, for free surface flows because gravity and inertia represent the most relevant forces. In free surface flow, under certain circumstances, the minor influence of the other forces (e.g., viscosity and surface tension) can increase to the point where they are no longer negligible and Froude scaling results in discrepancies between the model and prototype hydraulic behavior. This phenomenon is referred to as scale effects. Thus, a

[1]Ph.D. Student, Unit Research of Urban and Environmental Engineering, Research Group of Hydraulics in Environmental and Civil Engineering, Univ. of Liege, Quartier Polytech, Allée de la Découverte 9, Bat B52/3 +1, B-4000 Liège, Belgium (corresponding author). Email: m.lodomez@uliege.be

[2]Professor, Utah Water Research Laboratory, Dept. of Civil and Environmental Engineering, Utah State Univ., 8200 Old Main Hill, Logan, UT 84322-8200. ORCID: https://orcid.org/0000-0001-6643-9436. Email: blake.tullis@usu.edub

[3]Professor, Unit Research of Urban and Environmental Engineering, Research Group of Hydraulics in Environmental and Civil Engineering, Univ. of Liege, Quartier Polytech, Allée de la Découverte 9, Bat B52/3 +1, B-4000 Liège, Belgium. Email: B.Dewals@uliege.be

[4]Research Associate, Unit Research of Urban and Environmental Engineering, Research Group of Hydraulics in Environmental and Civil Engineering, Univ. of Liege, Quartier Polytech, Allée de la Découverte 9, Bat B52/3 +1, B-4000 Liège, Belgium. Email: pierre.archambeau@uliege.be

[5]Professor, Unit Research of Urban and Environmental Engineering, Research Group of Hydraulics in Environmental and Civil Engineering, Univ. of Liege, Quartier Polytech, Allée de la Découverte 9, Bat B52/3 +1, B-4000 Liège, Belgium. Email: michel.pirotton@uliege.be

[6]Associate Professor, Unit Research of Urban and Environmental Engineering, Research Group of Hydraulics in Environmental and Civil Engineering, Univ. of Liege, Quartier Polytech, Allée de la Découverte 9, Bat B52/3 +1, B-4000 Liège, Belgium. Email: S.Erpicum@uliege.be

Note. This manuscript was submitted on June 26, 2018; approved on January 4, 2019; published online on April 9, 2019. Discussion period open until September 9, 2019; separate discussions must be submitted for individual papers. This paper is part of the ***Journal of Hydraulic Engineering***, © ASCE, ISSN 0733-9429.

main challenge of laboratory-scale physical modeling lies in the identification and understanding of the resulting scale effects (Heller 2011).

A review of the literature found only one study addressing scale effect and nappe oscillation. Anderson and Tullis (2018) found that smaller scale linear weir models exhibited more temporal variability and irregularity as well as a hysteretic behavior relative to larger (non-geometrically similar) linear weir models. This study also implied that nappe oscillation may not scale with Froude similarity because nappe oscillation occurred for a common range of unit discharge (q) at both model scales. In an effort to better understand the scaling of nappe oscillations, a new study has been undertaken to assess the nappe oscillation occurrence and characteristics on two geometrically similar laboratory-scale facilities with a size scale factor of 3 regarding the fall height and weir geometry.

Experimental Setups

Testing Facilities

Model 1 was a prototype-scale linear weir (Fig. 1), constructed and evaluated at the Engineering Hydraulics Laboratory at the University of Liège (Belgium). This facility included an elevated headbox that provided flow to two identical weirs (3.5-m-long crest and a 3.0-m-high chute) installed in parallel, with only one weir tested at a time. In the framework of this study, only the one constructed with two sidewalls and a backwall to investigate a confined nappe with a nonvented air cavity behind the nappe (on the right in Fig. 1) was used. Flow to the headbox was provided by two pumps with a combined maximum flow capacity of 0.25 m^3/s, measured with an electromagnetic flowmeter with an accuracy of 0.5%. Inflows passed through a diffuser and a baffle to establish tranquil uniform approach flows to either weir.

Model 2, which was tested at the Utah Water Research Laboratory (UWRL) at Utah State University, featured a 4.70-m-long, 1.20-m-wide, and 1.20-m-deep rectangular flume (Fig. 2). The flume was supplied with water via a 0.3-m-diameter pipe containing a calibrated venturi flowmeter (±0.25% accuracy). A baffle wall was placed near the upstream end of the flume to minimize the turbulence and improve flow straightening. The linear weir supported by a wooden frame was set up 3.5 m downstream from the flume inlet. The fall height was 1.0 m and confined by two sidewalls (acrylic) and a back wall (wood).

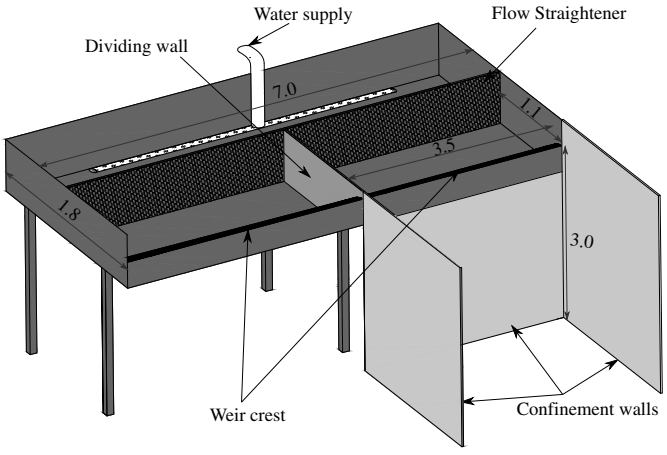

Fig. 1. Model 1 schematic facility. Dimensions in meters.

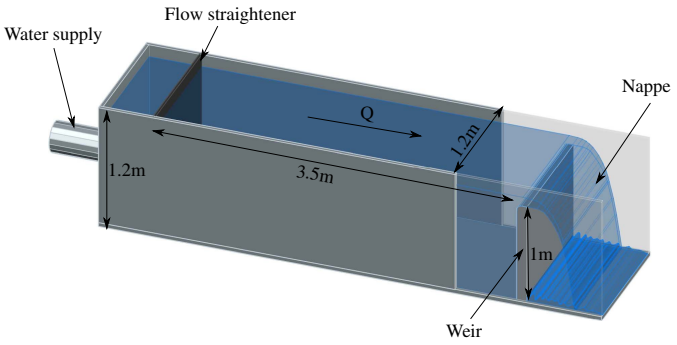

Fig. 2. Model 2 schematic facility.

Models 1 and 2 were geometrically similar (1:3). Two crest profiles were tested: a quarter-round (QR) and a truncated half-round (THR) (Fig. 3). The crest radii (R) for Models 1 and 2 were 150 and 50 mm, respectively. Weir flow experiments at both model scales were limited to confined nappe-flow conditions.

Instrumentation

A free-field microphone [MC212 (Model 1), Metravib, Limonest, France and Behringer ECM8000 (Model 2), Behringer GmbH, Willich, Germany] and a high speed-camera (GoPro Hero 4, GoPro, San Mateo, CA), placed in the centerline of the weir, were used to document the nappe oscillations occurrence and their associated frequencies. Sound recording and analysis supported the detection of the oscillations and provided, for nappe oscillation cases, two sound characteristics: the dominant noise frequency and its magnitude. Details of the method can be found in Lodomez et al. (2018c). The absolute sound intensities of Models 1 and 2 could not be compared because the sound signals were recorded in different acoustic environments. The absolute thresholds defining the occurrence of nappe oscillation were therefore different. To compare the models, the sound intensity of each test was normalized by the maximum intensity of the tested configuration.

The high-speed camera (240 Hz) captured the visible horizontal bands of the falling water. Fig. 4 illustrates these bands for Model 1 (THR crest shape and a unit discharge, q, of 0.03 m^2/s) and their propagation along the nappe in the direction of flow. The frequency of these visible oscillations was determined according to the method developed in Lodomez et al. (2018c). As shown in Lodomez et al. (2016a, b, 2018c), the frequencies gained from

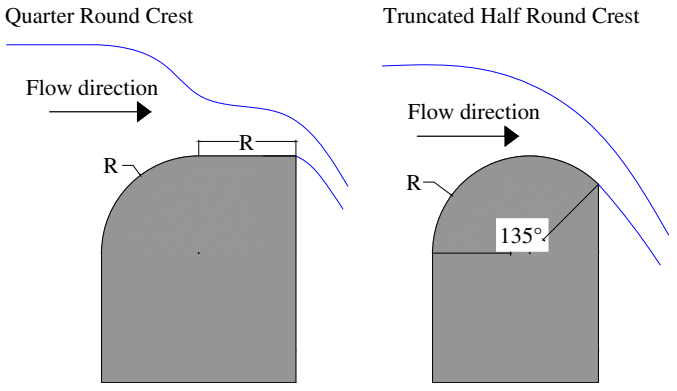

Fig. 3. Quarter-round and truncated half-round crest profiles, with the radius (R) for Models 1 and 2, respectively, equal to 0.15 and 0.05 m.

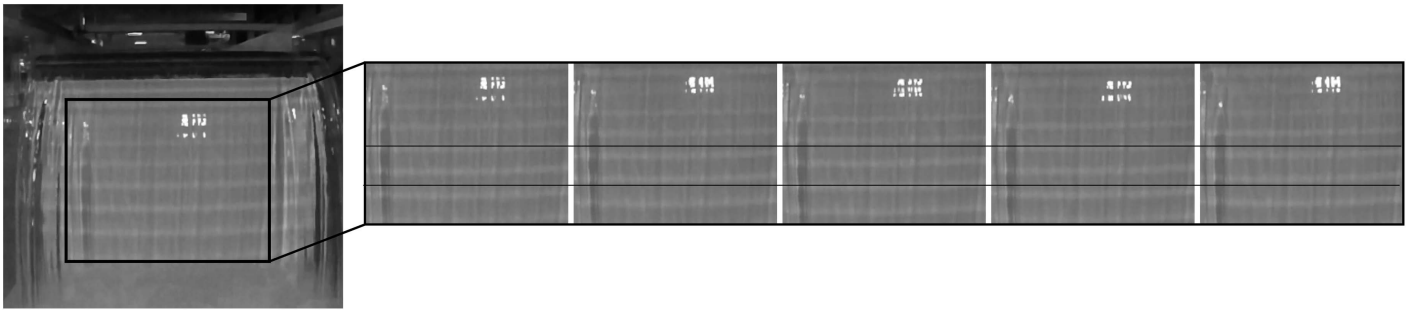

Fig. 4. Downstream view of on oscillation nappe. Tracking of the oscillations along the nappe in a set of five successive images with 8.33×10^{-3} s between two successive images.

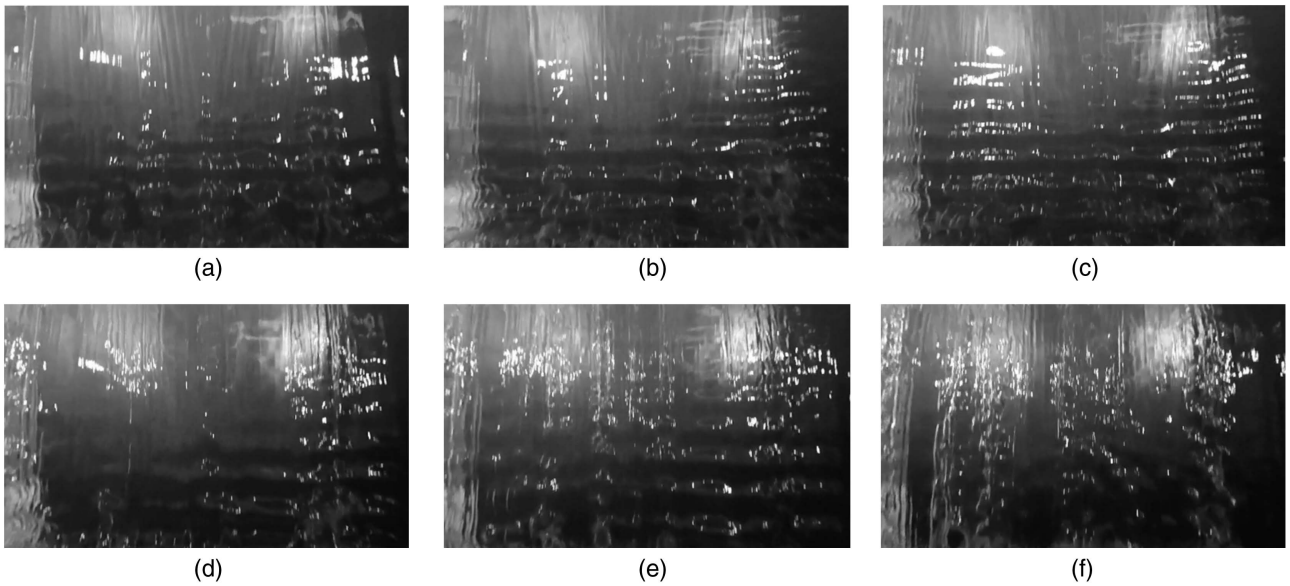

Fig. 5. Nappe characteristics for Model 1 and QR crest profile: (a) $q = 0.01$ m^2/s; (b) $q = 0.02$ m^2/s; (c) $q = 0.03$ m^2/s; (d) $q = 0.04$ m^2/s; (e) $q = 0.05$ m^2/s; and (f) $q = 0.06$ m^2/s.

image and sound analyses are identical. In the following, nappe oscillation frequencies are quantified without distinction between the two detection methods.

Results

Quarter-Round Crest Profile

The flow range affected by nappe oscillations for Model 1 and QR crest profile was found to be 0.01–0.055 m^2/s, with higher sound disturbances between 0.025 and 0.045 m^2/s, as confirmed by the visual nappe characteristics and sound intensity in Figs. 5 and 6(a). Indeed, although a substantial decrease of the sound level was observed for $q = 0.05$ m^2/s, horizontal waves were visible up to $q = 0.055$ m^2/s. The frequencies of the nappe oscillations in this configuration were between 31.5 and 35.5 Hz [Fig. 6(b)]. Nappe oscillations typically occurred in a steady-state fashion, showing little to no temporal fluctuation in behavior (e.g., starting and stopping, changes in amplitude) when present.

According to Froude similitude, the flow range leading to nappe oscillations in Model 1 (0.01–0.055 m^2/s) would correspond to 0.002–0.011 m^2/s for Model 2. However, for these discharges, nappe oscillations were not detected for Model 2. In addition, nappes tend to break up at such low discharges. In particular, the nappe break-up length is less than the Model 2 fall height (1 m) for $q < 0.004$ m^2/s according to Horeni's formula (Ervine et al. 1997; Castillo et al. 2014). In contrast, nappe oscillations were observed in Model 2 between 0.015 and 0.06 m^2/s, while the flow range that generated high noise disturbance was only between 0.015 and 0.03 m^2/s [Fig. 6(a)]. For higher discharges, a continuous decrease of the sound intensity was observed. In parallel, Fig. 7 illustrates the horizontal bands that characterized the nappe oscillations in particular between 0.015 and 0.04 m^2/s. For higher discharges, these bands were visible at the crest but seemed to vanish during the fall. Based on sound and image analyses, frequencies varying from 48.85 to 36.5 Hz for q lower than 0.03 m^2/s were detected. For higher q, several frequencies coexisted at the same time as shown by the audio spectrum in Fig. 8. These frequencies were equal to 34.25, 36.5, 38.85, 41.3, and 42.85 Hz for $q = 0.04$ m^2/s [Fig. 6(b)]. In addition, a hysteretic behavior was observed for q smaller than 0.02 m^2/s. Indeed, for increasing discharges, the oscillating nappes experienced intermittent periods of nappe stability. Oscillating periods lasting approximately 20–50 s

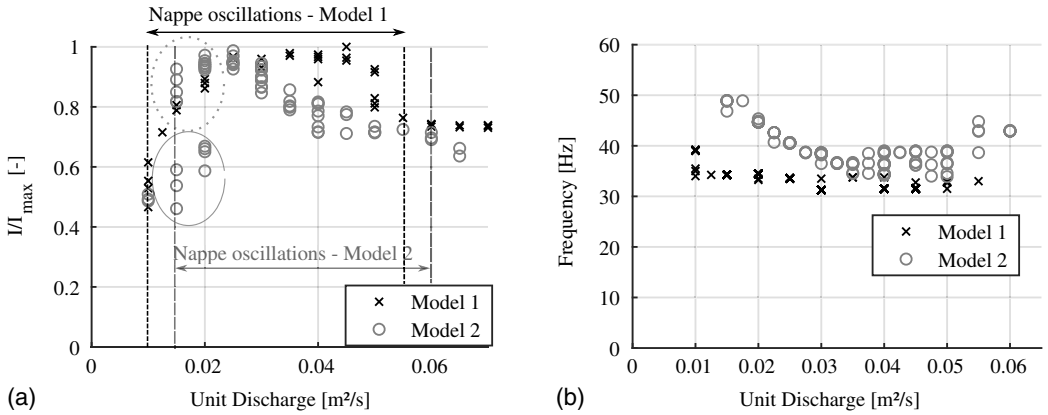

Fig. 6. (a) Results of sound analysis for the QR crest profiles. Hysteresis behavior for Model 2 illustrated by oscillating data (dotted circle) and no oscillating data (solid circle); and (b) frequencies of nappe oscillations.

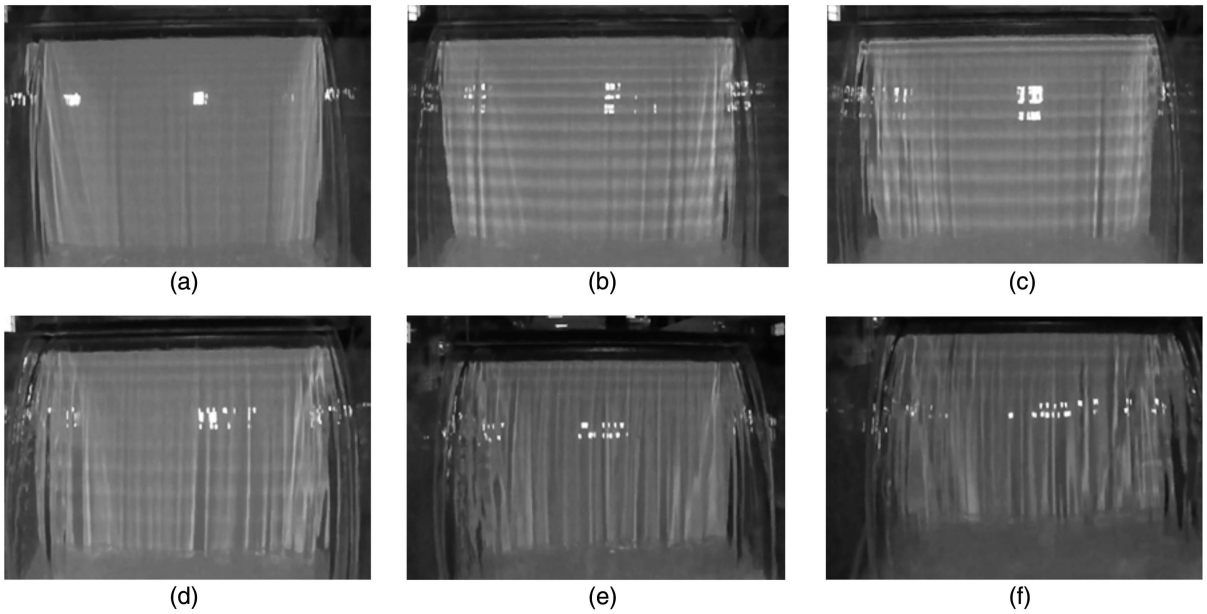

Fig. 7. Nappe characteristics for Model 2 and QR crest profile: (a) $q = 0.015$ m^2/s; (b) $q = 0.02$ m^2/s; (c) $q = 0.03$ m^2/s; (d) $q = 0.04$ m^2/s; (e) $q = 0.05$ m^2/s; and (f) $q = 0.06$ m^2/s.

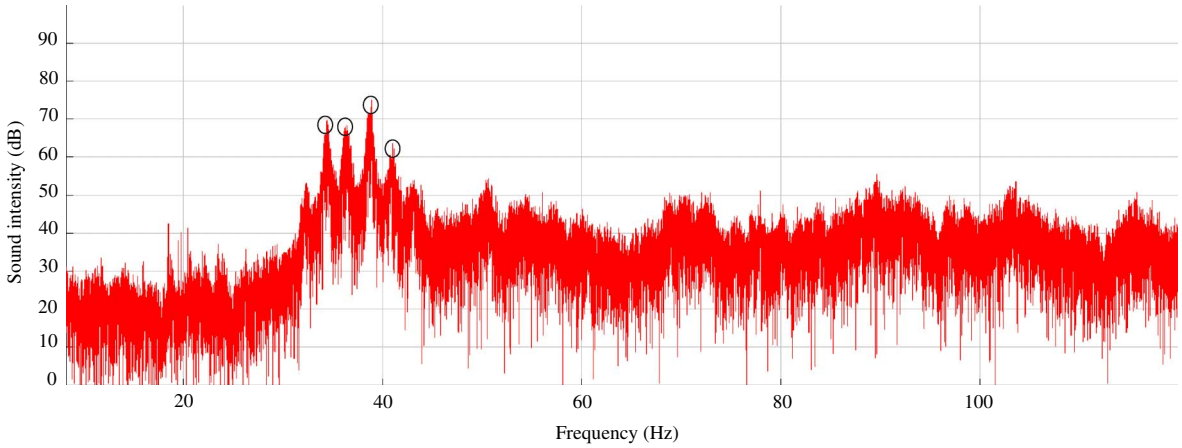

Fig. 8. Audio spectrum for Model 2, QR crest profile, and $q = 0.04$ m^2/s.

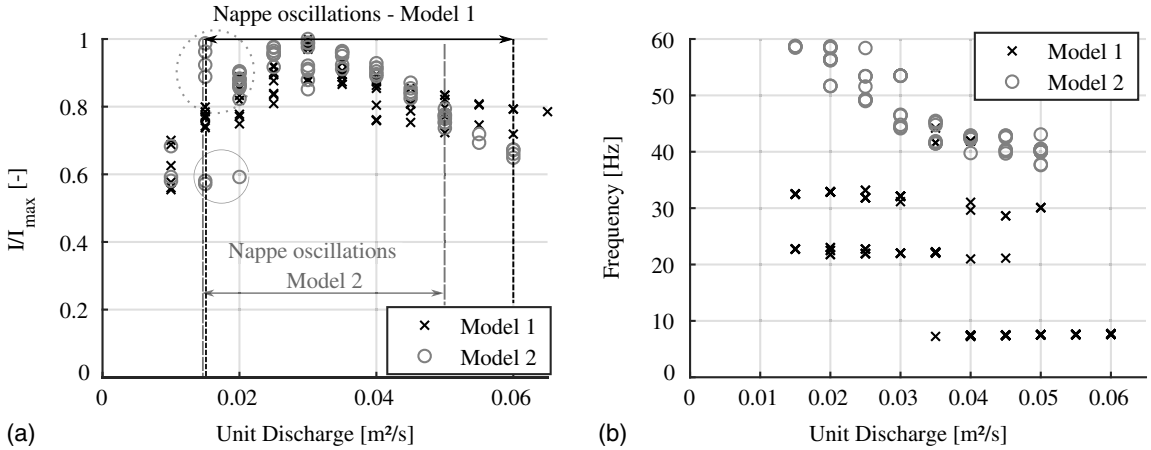

Fig. 9. (a) Results of sound analysis for the THR crest profiles. Hysteresis behavior for Model 2 illustrated by oscillating data (dotted circle) and no oscillating data (solid circle); and (b) frequencies of nappe oscillations.

were observed at a frequency of approximately 5 min. In contrast, for decreasing discharge from an oscillating unit discharge ($q > 0.2$ m^2/s), oscillations were temporally constant.

Truncated Half-Round Crest Profile

With the THR crest installed in Model 1, nappe oscillations were detected between 0.015 and 0.06 m^2/s. Nappe oscillation noise production increased with increasing q, peaked at $q = 0.03$ m^2/s, and then showed a gradual decrease as q continued to increase [Fig. 9(a)]. The visual characteristics of nappe oscillations, reported in Fig. 10, illustrate clear horizontal bands for $q < 0.04$ m^2/s. For higher q, horizontal waves still existed but were disordered and finally vanished. Although nappe oscillations were not visually detectable due to their phase shift, image analysis detected a frequency pattern of 7.25–8 Hz until $q = 0.06$ m^2/s [Fig. 9(b)]. This frequency was also detected with the audio spectrum. In parallel, for $q < 0.04$ m^2/s, two particular frequencies, i.e., ≈22 and ≈32 Hz, were simultaneously detected by sound and image analysis. These particular frequencies seem to be harmonics of the small frequency (≈7.25–8 Hz) detected for the higher q. As illustrated in Fig. 9(b), harmonics were also discerned by sound and image analysis for 0.035, 0.04, 0.045, and 0.05 m^2/s.

In the same way as for the QR profile, no oscillation was observed in Model 2 for the scaled q range of Model 1, i.e., between 0.003 and 0.012 m^2/s. Nonetheless, nappe oscillations were detected in Model 2 between 0.015 and 0.05 m^2/s. High levels of sound intensity were recorded for $0.015 < q < 0.03$ m^2/s with a maximum intensity for $q = 0.03$ m^2/s [Fig. 9(a)]. Then, for $q > 0.03$ m^2/s, a continuous decrease of the intensity was observed. In parallel, Fig. 11 illustrates the horizontal bands that characterized the nappe oscillations in particular between 0.02 and 0.04 m^2/s and their disappearance for $q > 0.05$ m^2/s. The frequencies of the nappe oscillations varied from 58.75 to 37.65 Hz

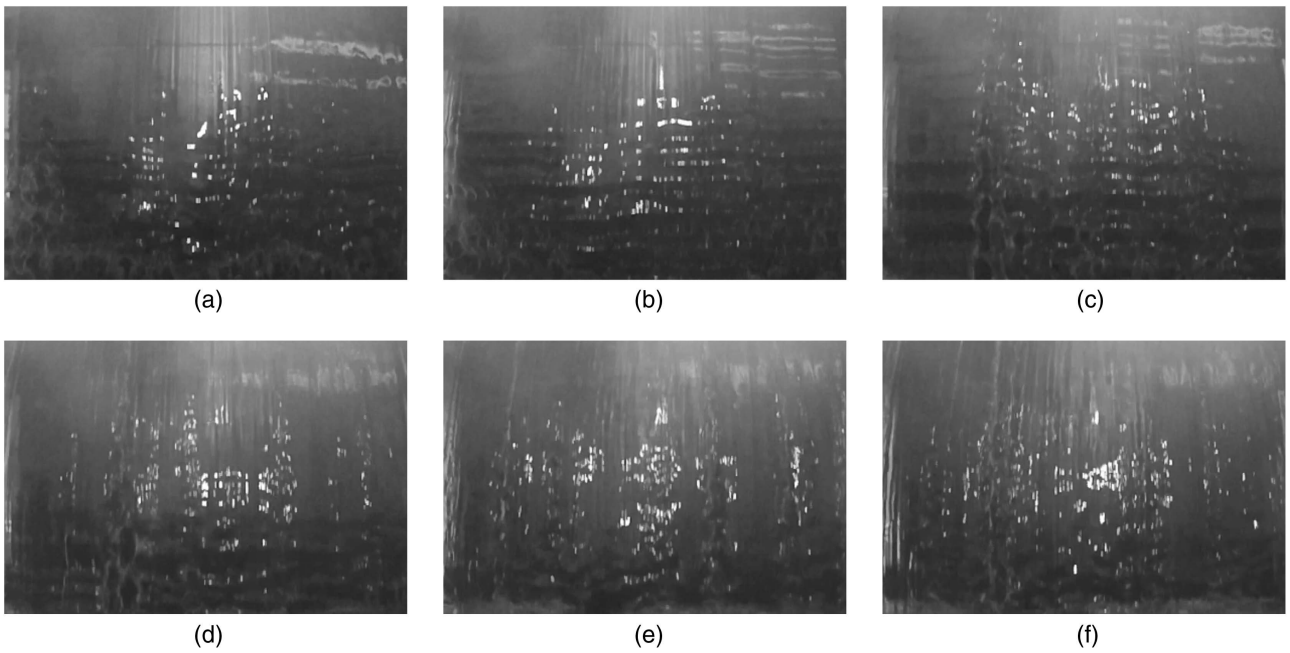

Fig. 10. Nappe characteristics for Model 1 and THR crest profile: (a) $q = 0.01$ m^2/s; (b) $q = 0.02$ m^2/s; (c) $q = 0.03$ m^2/s; (d) $q = 0.04$ m^2/s; (e) $q = 0.05$ m^2/s; and (f) $q = 0.06$ m^2/s.

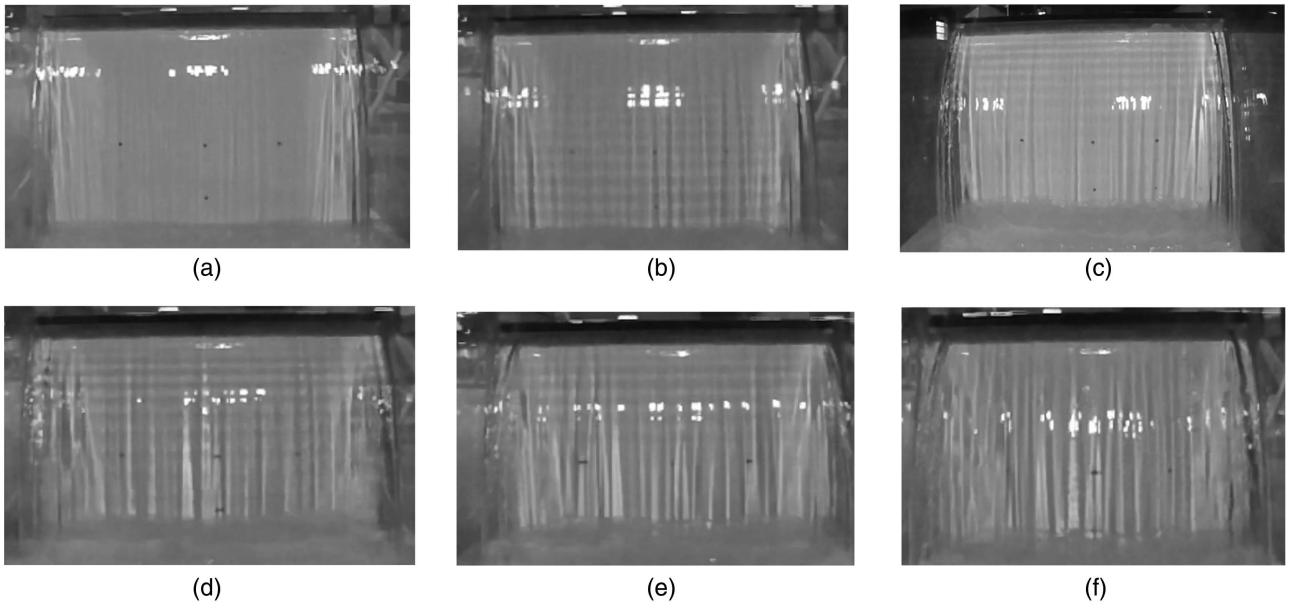

Fig. 11. Nappe characteristics for Model 2 and THR crest profile: (a) $q = 0.01$ m^2/s; (b) $q = 0.02$ m^2/s; (c) $q = 0.03$ m^2/s; (d) $q = 0.04$ m^2/s; (e) $q = 0.05$ m^2/s; and (f) $q = 0.06$ m^2/s.

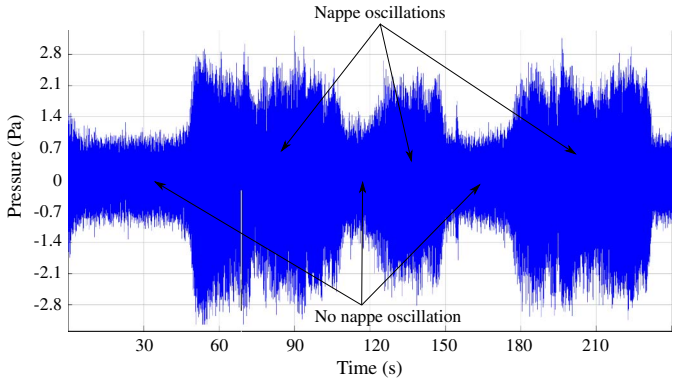

Fig. 12. Time evolution of the air pressure signal (sound signal recorded by the microphone) for Model 2, THR crest profile, and $q = 0.03$ m^2/s. Alternation of oscillating and nonoscillating behavior along time.

based on sound and image analysis. The highest frequencies were observed between 0.015 and 0.03 m^2/s with a decrease in that range from 58.75 to 44.15 Hz [Fig. 9(b)]. Then for higher q, a stabilization of the frequency was observed with frequencies varying from 44.15 to 37.65 Hz. For $q = 0.015$ and 0.02 m^2/s, nappe oscillations showed a hysteretic behavior. With these conditions, nappe oscillation occurrence was dependent upon the unit discharge prior to changing the flow. In addition, some temporal variability was observed for this configuration as illustrated in Fig. 12 based on the air pressure (sound) measurement.

Discussion

The first key finding of this research is that the nappe oscillations always appeared in the same range of unit discharge independent of size scale. The occurrence of nappe oscillations was indeed observed, for both facilities and crest shape, between 0.015 and 0.05 m^2/s approximately. This suggests that the nappe oscillation phenomenon cannot be scaled according to Froude similitude and is thus not driven solely by gravity and inertia.

Within this flow range, oscillation characteristics were slightly affected by the model scale. In particular, the sound intensity evolution as a function of q varied. For the QR crest profile weir tests, a clear decrease in sound intensity was observed for $q > 0.45$ m^2/s in the larger model (Model 1), while a more gradual decrease was observed for the smaller model (Model 2). For the THR crest profile, Model 1 produced a slight dampening of the sound intensity between 0.03 and 0.04 m^2/s and then reached a stabilized sound level for $q > 0.04$ m^2/s; Model 2 produced continuously decreasing sound levels for $q > 0.03$ m^2/s. The frequencies of the nappe oscillations also varied with model size. For a QR crest profile, the Models 1 and 2 frequencies varied for $q < 0.03$ m^2/s and became similar for $q > 0.03$ m^2/s. For the THR, Models 1 and 2 frequencies were completely different except for three tests at $q = 0.035$ and 0.04 m^2/s.

The second observation concerns the variability of the nappe oscillations and their frequencies. The smaller model (Model 2) results showed substantially more variation in the nappe oscillation characteristics than the larger model (Model 1). Specifically, nappe oscillations with the smaller model were more inclined to exhibit temporal fluctuations in that periodically the nappe oscillations would stop for a short period of time and then start up again. With the larger model, nappe oscillations were temporally stable. Second, the variability also concerned the frequencies of these oscillations and the coexistence of various frequencies at the same time. Finally, hysteresis was observed with respect to nappe oscillation in the smaller model, while no hysteresis was observed in the larger model. These findings are in agreement with the first investigations on nappe oscillation scaling in Anderson and Tullis (2018).

In view of the variability of the nappe oscillation behavior between the models, an additional configuration was tested. This configuration, called Model 3, was Model 1 with a reduced fall height of 1 m and a THR crest profile, i.e., the fall height of Model 2. For this configuration, nappe oscillations were detected

J. Hydraul. Eng., 2019, 145(6): 04019022

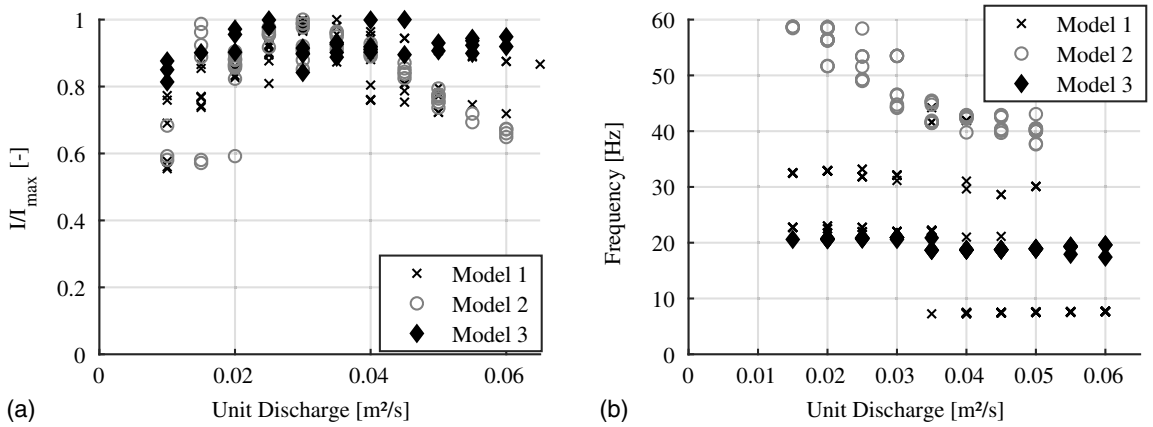

Fig. 13. (a) Results of sound analysis for the THR crest profiles; and (b) frequencies of nappe oscillations.

between 0.015 and 0.06 m^2/s, i.e., a similar q range as for Models 1 and 2. By comparison with other configurations, sound intensity evolution with q, illustrated in Fig. 13(a), varied less. However, the typical increase of sound intensity was observed for $0.015 < q < 0.025$ m^2/s followed by a drop of the intensity, which characterized the reduction of the nappe oscillations for $0.03 < q < 0.06$ m^2/s. Nevertheless, the detection of two maximum intensities for $q = 0.04$ and 0.045 m^2/s demonstrate the existence of the oscillations for these q. Dominant frequencies in the audio spectrum were therefore detectable between 0.015 and 0.06 m^2/s. These were identical to the horizontal band frequencies and varied from 17.4 to 20.6 Hz [Fig. 13(b)].

The five configurations tested in this study led to several findings. By comparing the configurations with an identical fall height and a different crest profile, i.e., Model 2 QR, Model 2 THR, and Model 3, or Model 1 QR and Model 1 THR, it is found that the frequencies of the oscillations were different. Although some similar frequencies (≈32–35 Hz) were observed for Models 1 and an identical frequency behavior (decrease from 58 to 40 Hz) was observed for Model 2, the oscillation frequency of Model 3, different from the ones of Model 2, shows that the frequencies depend on the crest profile. In addition, experiments for the Model 1 THR profile identified the existence of harmonics, which was not observed for the other profile. This shows that the profile of the crest affects the appearance of the oscillations and their characteristics. The crest widths in the transverse direction of Models 2 and 3 are different. However, Lodomez et al. (2017) showed that frequencies of the oscillations were not affected by a modification of the width, which allowed the comparison of these two data sets. The comparison of the configurations with an identical crest profile and a different fall height, i.e., Model 1 THR and Model 3, indicates that the fall height impacts the frequencies of the oscillations and the evolution of their intensity. This finding is in accordance with the findings of Schmid and Henningson (2002), who show a variation of the oscillation frequency of a vertical thin nappe with its fall height.

In an effort to better understand the impact of model dimension and parameters on the oscillation frequency, a dimensionless frequency f_{ad} was defined by the following equations (Lodomez et al. 2018c):

$$f_{ad} = \frac{q}{fe^2} \tag{1}$$

with e = characteristic dimension of the nappe (m); and f = nappe oscillation frequency (1/s). This characteristic dimension, e, was computed as the nappe thickness at impact, calculated from the downward velocity of the water sheet at impact $V(L)$ (m/s) (Casperson 1993)

$$e = \frac{q}{V(L)} = \frac{q}{\sqrt{V_0^2 + 2gL}} \tag{2}$$

where L = chute height (m); g = gravitational acceleration (m/s^2); and V_0 = vertical velocity component of the nappe leaving the crest (m/s). For the QR crest, the initial vertical velocity was assumed equal to 0, while for the THR crest V_0 was deduced from nappe thickness, experimentally measured, and then projected according to the angle of the weir crest at the downstream end (45° with horizontal). Fig. 14 shows the dimensionless frequencies obtained as a function of the Reynolds number, $\mathrm{R} = q/\nu$, with ν being the kinematic viscosity, for the five data sets. First, the variability of the frequencies by the occurrence of harmonics for the data set of Model 1 THR is clearly visible. Second, the impact of the crest shape and the fall height, discussed previously, is illustrated in particular with the comparison of the data gained for Model 3, Model 1 QR, and Model 1 THR. Finally, the impact of the scaling is visible by the clear difference of dimensionless frequencies observed for Models 1 and 2.

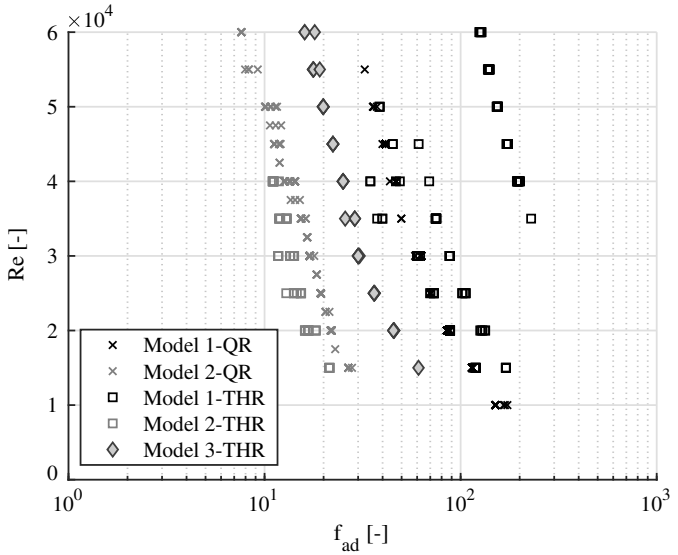

Fig. 14. Dimensionless frequency of nappe oscillation for all data of this study.

Conclusions

This experimental study investigated the possible size scale effects on nappe oscillations. The nappe oscillation occurrence assessment and frequency evaluation were performed using sound and image analyses for two experimental facilities, i.e., a prototype-scale linear weir (3-m fall height) and a scale model (1:3) of the same weir (1-m fall height). Experiments showed that nappe oscillations cannot be scaled according to the traditional similarity for free-overfall structure, i.e., Froude similitude. Indeed, the nappe oscillations always appeared in approximately the same unit discharge range (0.015–0.05 m^2/s), independent of the weir size scale and the test facility.

This research also indicated that nappe oscillation development and characteristics (intensity and frequencies) are affected by fall height and crest profile. In particular, experiments pointed out that the crest profile modified the oscillation frequencies, while the fall height impacted both the frequencies and the sound intensity evolution. In addition, for a fall height of 1 m and $q < 0.02$ m^2/s, a hysteretic behavior and a variability of the oscillation in time were observed. Finally, this study shows that nappe oscillations may appear on free-overfall structures, with a quarter-round or a truncated half-round crest profile, for $0.015 \leq q \leq 0.05$ m^2/s independent of the structure size (for the range of weir sizes tested).

The results presented in this study are specific to the five tested geometries. Additional studies are needed to better understand the detailed effect of the crest profile, the fall height, and the width of the weir on the nappe oscillation characteristics.

Acknowledgments

The first author acknowledges the Fédération Wallonie-Bruxelles for the funding of hers research stay in Utah.

Notation

The following symbols are used in this paper:

e = characteristic length (m);
f = oscillation frequency (1/s);
f_{ad} = dimensionless frequency;
g = gravitational acceleration (m/s^2);
I = maximum sound intensity of audio spectrum for a given configuration and a unit discharge (dB);
I_{max} = maximum sound intensity of audio spectrum for a given configuration in the unit discharge range affected by nappe oscillations (dB);
L = fall height (m);
q = specific discharge (m^2/s);
R = Reynolds number;
V_0 = initial vertical velocity (m/s);
$V(L)$ = vertical velocity of the water sheet at impact (m/s); and
ν = kinematic viscosity (m^2/s).

References

Anderson, A., and B. P. Tullis. 2018. "Finite crest length weir nappe oscillation." *J. Hydraul. Eng.* 144 (6): 04018020. https://doi.org/10.1061/(ASCE)HY.1943-7900.0001461.

Binnie, A. 1972. "The stability of a falling sheet of water." *Proc. R. Soc. London, Ser. A: Math. Phys. Eng. Sci.* 326 (1565): 149–163. https://doi.org/10.1098/rspa.1972.0002.

Casperson, L. W. 1993. "Fluttering fountains." *J. Sound Vibr.* 162 (2): 251–262. https://doi.org/10.1006/jsvi.1993.1117.

Castillo, L. G., J. M. Carrillo, and Á. Sordo-Ward. 2014. "Simulation of overflow nappe impingement jets." *J. Hydroinf.* 16 (4): 922–940. https://doi.org/10.2166/hydro.2014.109.

Chanson, H. 1996. *Some hydraulic aspects during overflow above inflatable flexible membrane dam*. Rep. No. CH47/86. Brisbane, Australia: Univ. of Queensland.

Crookston, B. M., A. Anderson, L. Shearin-Feimster, and B. P. Tullis. 2014. "Mitigation investigation of flow-induced vibrations at a rehabilitated spillway." In *Proc., 11th National Conf. on Hydraulics in Civil Engineering and 5th Int. Symp. on Hydraulic Structures: Hydraulic Structures and Society-Engineering Challenges and Extremes*, 149–156. Barton, Australia: Engineers Australia.

Ervine, D. A., H. T. Falvey, and W. Withers. 1997. "Pressure fluctuations on plunge pool floors." *J. Hydraul. Res.* 35 (2): 257–279. https://doi.org/10.1080/00221689709498430.

Ettema, R., R. Arndt, P. Roberts, and T. Wahl. 2000. *Hydraulic modeling: Concepts and practice*. Reston, VA: ASCE.

Heller, V. 2011. "Scale effects in physical hydraulic engineering models." *J. Hydraul. Res.* 49 (3): 293–306. https://doi.org/10.1080/00221686.2011.578914.

Lodomez, M., B. Bousmar, B. Dewals, P. Archambeau, M. Pirotton, and S. Erpicum. 2018a. "In-situ measurement and mitigation of nappe oscillations—The Papignies and Nisramont dams in Belgium." In *Proc., 7th IAHR Int. Symp. on Hydraulic Structures*. Logan, UT: Utah State Univ.

Lodomez, M., M. Pirotton, B. Dewals, P. Archambeau, and S. Erpicum. 2016b. "Frequencies of nappe vibration for free-overfall structures." In *Proc., 6th International Junior Researcher and Engineer Workshop on Hydraulic Structures (IJREWHS)*. Logan, UT: Utah State Univ.

Lodomez, M., M. Pirotton, B. Dewals, P. Archambeau, and S. Erpicum. 2016a. "Sustainable hydraulics in the era of global change." In *Proc., 4th IAHR Europe Congress*. Boca Raton, FL: CRC Press.

Lodomez, M., M. Pirotton, B. Dewals, P. Archambeau, and S. Erpicum. 2017. "Could piano key weirs be subject to nappe oscillations?" In *Proc., 3rd Int. Workshop on Labyrinth and Piano Key Weirs (PKW 2017)*, 135–144. Boca Raton, FL: CRC Press.

Lodomez, M., M. Pirotton, B. Dewals, P. Archambeau, and S. Erpicum. 2018c. "Nappe oscillations on free-overfall structures: Experimental analysis." *J. Hydraul. Eng.* 144 (3): 04018001. https://doi.org/10.1061/(ASCE)HY.1943-7900.0001420.

MWSDB (Metropolitan Water, Sewerage, and Drainage Board). 1980. *Investigation into spillway discharge noise at Avon Dam: ANCOLD bulletin no. 57*, 31–36. Sydney: MWSDB.

Sato, Y., S. Miura, T. Nagamine, S. Morii, and S. Ohkubo. 2007. "Behavior of a falling water sheet." *J. Environ. Eng.* 2 (2): 394–406. https://doi.org/10.1299/jee.2.394.

Schmid, P. J., and D. S. Henningson. 2002. "On the stability of a falling liquid curtain." *J. Fluid Mech.* 463: 163–171. https://doi.org/10.1017/S002211200200873X.

USBR (US Bureau of Reclamation). 1964. *Experience of the Bureau of Reclamation with flow-induced vibrations*. Rep. No. 538. Washington, DC: USBR.